Cellulose nanofibers from bamboo and their nanocomposites with polyvinyl alcohol: Preparation and characterization

Article *in* Polymer Composites · December 2016

DOI: 10.1002/pc.24249

6 authors, including:

Shenjie Han
Chinese Academy of Forestry
12 PUBLICATIONS **121** CITATIONS

SEE PROFILE

Qiufang Yao
Tongji University
32 PUBLICATIONS **102** CITATIONS

SEE PROFILE

Cellulose Nanofibers From Bamboo and Their Nanocomposites With Polyvinyl Alcohol: Preparation and Characterization

Shenjie Han,[1] Qiufang Yao,[1] Chunde Jin,[1,2] Bitao Fan,[1] Huanhuan Zheng,[1] Qingfeng Sun[1,2]
[1]*School of Engineering, Zhejiang Agricultural and Forestry University, Lin'an 311300, People's Republic of China*

[2]*Key Laboratory of Wood Science and Technology, Zhejiang Province, People's Republic of China*

Bamboo cellulose nanofibers (BCNFs) having an average diameter of 15.02 nm were isolated from moso bamboo by chemical pretreatments combined with subsequent ultrasonic treatments to remove the hemicellulose and lignin and split the cellulose bundle into BCNFs. The isolation of BCNF is proved by transmission electron microscope (TEM), FTIR, XRD, and thermal gravimetric analyzer (TGA) characterizations. The BCNF was used as the reinforcing agent in polyvinyl alcohol (PVA) along with crosslinking agents to prepare crosslinked nanocomposite aerogels. The resulting BCNF/PVA aerogel, treated with methyltrichlorosilane using a chemical vapor deposition technology, was rendered both hydrophobic and oleophilic. Scanning electron microscope (SEM), FTIR, and TGA results showed the characteristics of BCNF/PVA aerogels with or without silane coating. Finally, these low-density hybrid aerogels proved to be efficiently absorbing organic solvents (e.g., hexane) and oils (e.g., pump oil) with an excellent selectivity, thereby making them potentially useful for spilled oil recovery and environmental protection. POLYM. COMPOS., 00:000–000, 2016.

INTRODUCTION

Aerogels are ultra-light, highly porous solids with high surface areas and typically manufactured by forming a gel network, removing the solvent without causing any pore collapse [1]. Because of characteristics such as high porosity, high specific surface area, low dielectric properties, and low density, these porous aerogels are attractive for a wide ranges of applications as low dielectric substrates [2], thermal and acoustic insulation [3, 4], catalyst supports [5], and as building and construction materials [6]. Over the past decade, most aerogels were fabricated from silica [7] or pyrolyzed organic polymers [8]. However, they are often subjected to intrinsic brittleness, which thereby restricts their use in applications where both high flexibility and mechanical strength are needed. Therefore, there is a growing interest in searching excellent organic aerogels that possess less brittleness and more flexibility.

Recently, the increasing depletion of fossil resources and severe environmental pollution was attributed to the refining of petrochemical products have drawn interest to developing alternative and sustainable resources to take the place of petrochemical resources, particularly from reproducible woody biomass resources [9–11]. Bamboo, a very potentially renewable woody biomass resource of the future, has the strengths of high yield and short growth cycle. Currently, the area of bamboo was about 5,000,000 hectares, and that of moso bamboo was about 3,000,000 hectares widely cultivated in the south and west of China, with an annual yield of about 18,000,000 tons and was greater than all other kinds of bamboo [12]. Bamboo, a kind of natural lignocellulose plant, is made up of approximately 47% cellulose, 26% lignin, and others substrates. Cellulose is one of the most abundant, sustainable, and environmental friendly materials in nature and is biodegradable and biocompatible [13–16]. In the last few decades, cellulose nanofibers (CNFs) have been intensively studied because of their unique characteristics (e.g., high surface area-to-volume ratio, high surface area, high mechanical strength, and the nanoscale dimensions) [17–19]. The various methods of extracting high purified nanofibers from cellulosic materials can be classified as mechanical (e.g., cryogenic crushing [20], grinding [21], and high-pressure homogenization [22]), chemical (e.g., acid hydrolysis) [23], and biological treatments, (e.g., enzyme-assisted hydrolysis [24]), TEMPO-mediated

Correspondence to: Q. Sun; e-mail: qfsun@zafu.edu.cn or C. Jin; e-mail: jincd@zafu.edu.cn
Contract grant sponsor: Zhejiang Provincial Natural Science Foundation of China; contract grant number: LZ14C160001; contract grant sponsor: Scientific Research Foundation of Zhejiang A&F University; contract grant number: 2014FR077.
DOI 10.1002/pc.24249
Published online in Wiley Online Library (wileyonlinelibrary.com).

oxidation on the surface of microfibrils and subsequently mild mechanical treatment, synthetic and electrospinning methods [25], as well as the combination of two or several of the mentioned methods above. Among these mentioned methods above, the ultrasonic technique, regarded as one of the most powerful approach used for isolating CNFs, has been sufficiently investigated [26]. During the ultrasonic process, the energy is shifted to cellulose chains via a cavitation process, which involves the formation, growth, and violent collapse of cavities in water [27]. The aforementioned energy called sonochemistry is approximately 10–100 kJ/mol, which provide a particular platform to break gradually the intense cellulose interfibrillar hydrogen bonding and disintegrate the micron-sized purified cellulose fibers into CNFs [28]. Thus, the ultrasonic isolation technology may be generally applied to various biomass resources consisting of CNFs and other embedding matrixes [29]. Therefore, the BCNFs used in this study were extracted from moso bamboo by ultrasonic isolation technology.

In spite of their excellent properties, such as their ultralow density and deformability, CNF aerogels possess inferior strength and modulus [30]. The PVA, a relatively cheap polymer, possesses superior properties such as biodegradability and biocompatibility [31]. The PVA demonstrates robust hydrophilic and hydrogen bonding characteristics due to the hydroxyl groups present in per repeating molecular unit. It can react with a variety of types of functional groups and thus form chemically and/or physically crosslinked nanocomposite hydrogels [32]. Herein, this study reports organic aerogels from BCNFs and PVA via freeze-drying process, which could overcome these deficits. The obtained BCNF/PVA aerogel, modified with methyltrichlorosilane by means of a chemical vapor deposition process, became hydrophobic and oleophilic [31, 33–35]. The silane-treated BCNF/PVA aerogels showed desirable oleophilic absorption abilities, but strongly repelled water. As a consequence, this study gives a facile and inexpensive method to manufacture robust hydrophobic aerogels based on renewable and various natural resources (i.e., BCNFs), which have excellent absorption for oil and chemical spill/leak clean-up.

EXPERIMENTAL SECTION

Raw Materials

Mature culms of moso bamboo (*Phyllostachys pubescence*), aged 4 years, collected from Lin'an Country in Zhejiang Province, China. First, the culms of mature bamboo were ground into particles, and then the powder was screened to obtain a powder size between 60 and 80 mesh. Benzene, ethanol, acetic acid, potassium hydroxide, sodium chlorite, PVA (MW: 1800 g mol^{-1}) and other chemicals were of laboratory grade and used without further purification.

Removal of Wax, Lignin, and Hemicelluloses From Bamboo

Pure cellulose was extracted from moso bamboo culms. A three-step process was used to remove wax, lignin, and hemicelluloses in sequence from moso bamboo culms, referring to previous experiments [26, 36, 37]. Briefly, a certain amount of the original bamboo powder (OBP) was first treated with benzene/ethanol (2:1, vol/vol) by refluxing in a Soxhlet apparatus for 6 hr to remove waxes, pigments, and oils. Afterward, the dewaxed bamboo powder was transferred to acidified sodium chlorite at 75°C for 1 hr, which was repeated five times until the product turned to white. Then the delignified bamboo powder was treated with 2 wt% potassium hydroxide at 90°C to remove hemicelluloses, residual starch, pectin, and silica. In order to acquire highly purified cellulose, the products were further reacted with an acidified sodium chlorite solution at 75°C and then treated with 5 wt% potassium hydroxide at 90°C. After a series of chemical treatments, the sample was filtered and rinsed with distilled water until the residues were neutralized. The samples were kept in a water-swollen state during the whole chemical process to reduce the generation of strong hydrogen bonds among cellulose bundles after removing matrix components [27, 38, 39]. The detailed compositions of the bamboo powder used in this study were determined by using the standard method described by National Renewable Energy Laboratory (NREL) [40] and they were composed of cellulose (57.5%), acid insoluble lignin (21.4%), and hemicelluloses (22.5%).

Preparation of BCNF

After the chemical pretreatment, the purified bamboo cellulose fibers (PBCF) were uniformly dispersed in distilled water at ~0.5 wt% (wt/wt) solid content. Approximately, 300 mL of water slurry containing samples was then dispersed in a Sonifiers® Cell Disruptor/Homogenizer (JY98-IIID, Ningbo Scientz Biotechnology Co., Ltd., China) and equipped with a 1-cm^2-diameter cylindrical titanium alloy probe tip. Subsequently, ultrasonication was conducted at 60 kHz in frequency for 30 min at an output power of 1200 W to isolate the fibers in an ice/water bath and the ice was maintained throughout the entire ultrasonication process [27]. To separate the large bundles, the sonicated suspension was then centrifuged and slender nanofibrils were acquired from the supernatant fraction. The bundles of the nanofibrils, collected as sediments, were retreated by high intensity ultrasonication.

Preparation of Crosslinked PVA/BCNF Aerogels

The BCNF suspensions were subjected to solvent exchange from water to ethanol in three steps, followed by solvent exchange from ethanol to *tert*-butanol in three steps [41]. The resulting BCNF suspensions mixed with

 DOI 10.1002/pc

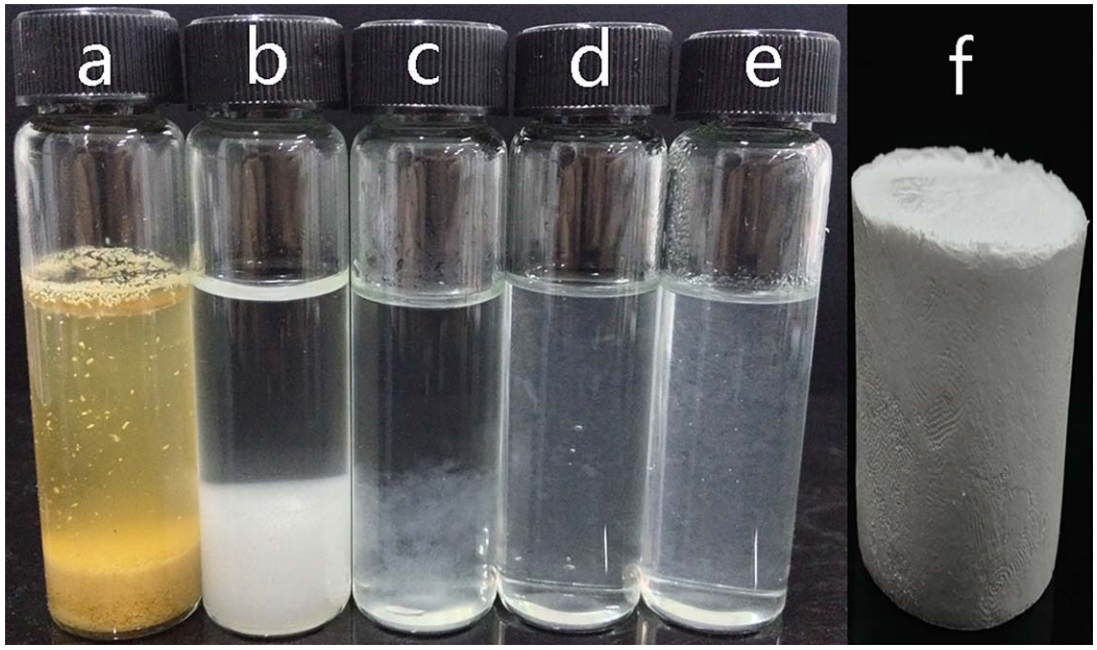

FIG. 1. Aqueous suspensions of the (a) OBP, (b) PBCF, (c) BCNF dispersion, (d) concentrated BCNF dispersion by solvent exchange, (e) mixture of BCNF and PVA, and (f) the prepared BCNF/PVA aerogel. [Color figure can be viewed at wileyonlinelibrary.com]

tert-butanol (the content of BCNF was 0.07%) stored at ambient temperature without any treatment.

PVA (1.0 g) was dissolved in 50 mL of the concentrated suspensions of BCNF and *tert*-butanol and stirred at 90°C for 40 min until the PVA was absolutely dissolved. Then, the mixture was sonicated in an ultrasonic bath for 1 hr and then placed in a vacuum oven to remove bubbles. After that, to reduce macroscopic fracture during the freezing process, the crosslinked hydrogel was first precooled at −30°C for 24 hr in a refrigerator. The resulting frozen hydrogel was freeze-dried using a Scientz-18 N freeze-dryer (Scientz Biotechnology, Ningbo, China). During the freeze-drying step, the cold trap temperature was below −55°C and the vacuum pressure was below 10 Pa. Finally, the obtained aerogel products were stored in a vacuum oven for further characterization. Figure 1 shows a scheme describing the procedures for fabricating crosslinked BCNF/PVA aerogels.

Preparation of Hydrophobic BCNF/PVA Aerogels

The hydrophobic BCNF/PVA aerogels were acquired by coating with methyltrichlorosilane via a chemical vapor deposition technique. The aerogels were stored in a vacuum desiccator. Then, a small glass bottle containing a certain amount of methyltrichlorosilane was placed into the vacuum desiccator together with the aerogels. The desiccator was sealed tightly and heated to 80°C in a vacuum-assisted oven for 12 hr. The aerogel and methyltrichlorosilane allowed to react for 24 hr at ambient temperature within the desiccator. The modified aerogels were kept in a vacuum desiccator under vacuum for 1 hr to eliminate the superfluous unreacted silane and the byproduct HCl.

Characterization Techniques

TEM specimens were prepared by depositing a 10-μL drop of a supernatant fraction of BCNF onto carbon-coated TEM grids (230-mesh copper, Beijing Zhongjingkeyi Technology Co., Ltd., China). The excess liquid was removed by blotting with a piece of filter paper after 10 min. After the samples had been completely dried, they were observed using an FEI Tecnai G2 electron microscope conducted at accelerating voltage of 80 kV.

X-ray diffraction (XRD) patterns of the OBP, PBCF, and BCNF were measured by XRD (Shimadzu LabX XRD-6000) operating with Cu Kα radiation ($\gamma = 1.5418$ Å) at a scan rate (2θ) of 2°/min with 40 kV accelerating voltage and the applied 30 mA current in the range of 5°–40°. The average values of cellulose crystallinity were calculated from the five samples. The crystallinity index (CrI) of the OBP, PBCF, and BCNF was determined using Eq. *1* given below:

$$\mathrm{CrI} = \left[\left(I_{002} - I_{\mathrm{amorph}}\right)/I_{002}\right] \times 100 \qquad (1)$$

This sentence has been moved in the method section.

FTIR spectra were recorded on a Fourier Transform infrared instrument (Nicolet Magna-IR 560, Thermo Scientific, USA) ranging from of 400 cm^{-1} to 4000 cm^{-1} with a 4 cm^{-1} resolution. The OBP, PBCF, and BCNF

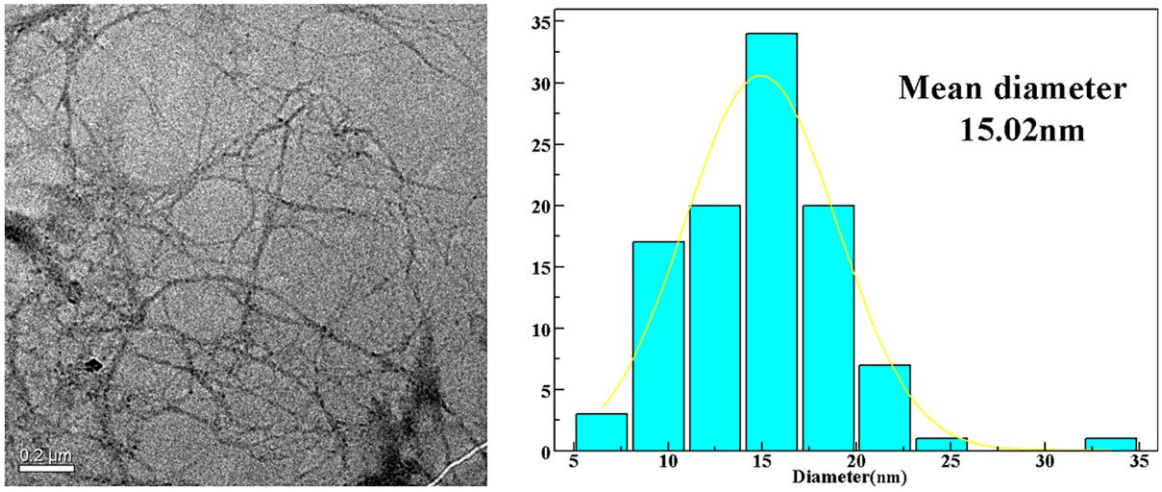

FIG. 2. TEM micrograph and diameter distribution of the BCNF. [Color figure can be viewed at wileyonlinelibrary.com]

were ground into powder using a fiber microtome and blended with KBr at 1:100, wt/wt sample: KBr ratio before pressing the mixture into ultrathin pellets.

SEM samples were prepared by placing the aerogels on a conductive carbon tape and sputter coating with gold. The characterization of BCNF/PVA aerogels were performed by using a Hitachi S-3400N instrument (S-3400N, Hitachi, Japan) at a 20.0 kV accelerating voltage of and a 5 mm working distance.

A PE-TGA7 thermogravimetric analyzer (Perkin Elmer Company) and a DTA/9050311 high temperature differential analyzer were employed to obtain the weight loss of freeze-dried samples. Each sample (~10 mg) was taken and measured in air, and then treated with 150 mL/min of dry pure N_2 with temperatures at the rate of 10°C/min in the range of 25–800°C.

The surface wettability of BCNF/PVA aerogels was studied by contact angle measurement via a contact angle analyzer (JC2000C) at ambient temperature. Water droplets of 5 μL were directly deposited at the top or bottom surfaces of the freeze-dried aerogel, and the water contact angles (WCAs) were measured. Five measurements were performed per aerogel at different surface locations and averaged. The contact angle was determined 10 s after the water droplets deposited and the tip used was a precision stainless tip.

RESULTS AND DISCUSSION

Schematic Illustration of BCNF/PVA Aerogels by Visual Examination

The fabrication process of BCNF/PVA aerogel is illustrated in Fig. 1. Typically, 2 g bamboo powder was subjected to successive chemical purification to obtain PBCF. As shown in Fig. 1, the yellow bamboo powder became white after chemical treatments, demonstrating that a mass of lignin was removed. After ultrasonic treatment, slender cellulose nanofiber was acquired from the supernatant fraction. Then the CNFs were converted to highly viscous suspensions by solvent exchange, a more colloidal structure was obtained. The combination of PVA and the concentrated suspensions by vigorous stirring was more viscous than the concentrated BCNF suspensions. Thereafter, the mixture was subjected to freeze-drying to generate BCNF/PVA aerogel.

Morphology of the BCNF

The morphology of BCNF was observed by TEM measurement (see Fig. 2). It is clearly shown that the BCNF possessed a fibrous structure with average dimensions of ~15.02 nm in diameter and several or even several hundred of microns in length. Such high aspect ratio made BCNF tend to form the web-like structure in the

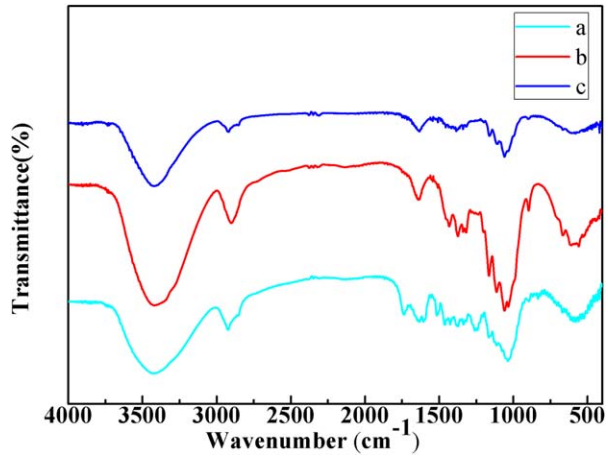

FIG. 3. FTIR spectra of the (a) OBP, (b) PBCF, and (c) BCNF. [Color figure can be viewed at wileyonlinelibrary.com]

 DOI 10.1002/pc

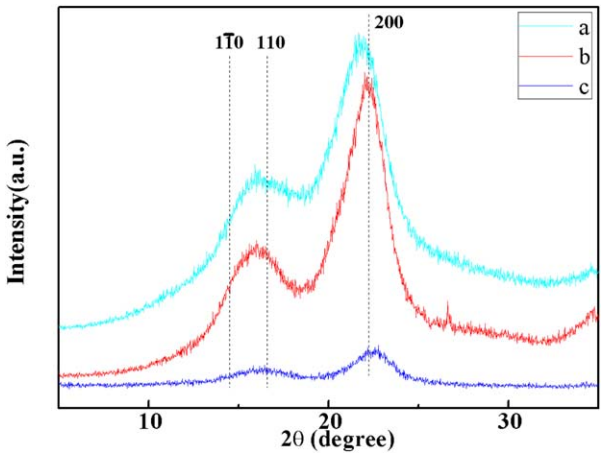

FIG. 4. X-ray diffraction patterns of (a) OBP, (b) PBCF, and (c) BCNF. [Color figure can be viewed at wileyonlinelibrary.com]

biocomposite, which was expected to improve the physical properties of PVA.

Analysis of FTIR and XRD Spectra

The changes of the physico-chemical properties of lignocellulosic materials during the different stage of treatment, starting from the OBP stage to the production of BCNF, were characterized by FTIR. The FTIR spectra of the OBP, PBCF, and BCNF were analyzed to confirm the various chemical components in Fig. 3. The OBP gives a relatively low intensity absorbance at 3413 and 1638 cm^{-1}. These peaks are responsible for the OH-bending and OH-stretching frequencies, respectively. In the OBP, the hydroxyl groups are bound by other cementing materials like lignin, waxes, and hemicelluloses and hence its peaks are not exposed in the FTIR spectrum [42]. After a series of chemical treatments, the prominent peak of the OBP at 1732 cm^{-1}, which is attributed either to the acetyl and uronic ester groups of the hemicellulose or to the ester linkage of the carboxylic groups of the ferulic and *p*-coumeric acids of lignin and/or hemicellulose [43, 44], disappeared completely in the PBCF, indicating the removal of most of the hemicelluloses and lignin from the OBP. Compared with the OBP, the intensity of the 1508 cm^{-1} peak represents the –C═C– stretch of the aromatic rings of lignin disappeared in the PBCF, which is attributed to the removal of lignin [40, 43]. Although the peak at 1638 cm^{-1}, linked with the H—O—H stretching vibration of absorbed water in carbohydrates, declined in the OBP, it could also be detected in the purified cellulose fibers. This indicates that a small quantity of hemicellulose still exists in the PBCF, which plays an active role in the facilitation of nanofibrillation. The peak at 896 cm^{-1}, associated with the C—H rock vibration of cellulose (anomeric vibration, specific for β-glucosides), shows an increasing tendency with a series of chemical pretreatments indicating the removal of tightly bound cementing materials and exposure of the pure cellulosic fibers [42].

The crystallinity of the OBP, PBCF, and BCNF has been investigated by X-ray diffractometry. All the samples demonstrated sharp diffraction peaks around $2\theta = 14.5°$ (110), 16.5° (1 $\bar{1}$0) and 22.3° (200) [45], which were supposed to represent the typical cellulose-I structure [46]. This indicated that the crystal integrity was unchanged during chemical purification and ultrasonic treatment. From the XRD data (Fig. 4), The CrI was estimated as 42.34, 60.87, and 58.73% for the OBP, PBCF, and BCNF, respectively. The increase in crystallinity from 42.34% for the OBP to 60.87% for the PBCF was undoubtedly attributed to the removal of hemicellulose and lignin in amorphous regions, which led to the realignment of cellulose molecules. After ultrasonic treatment,

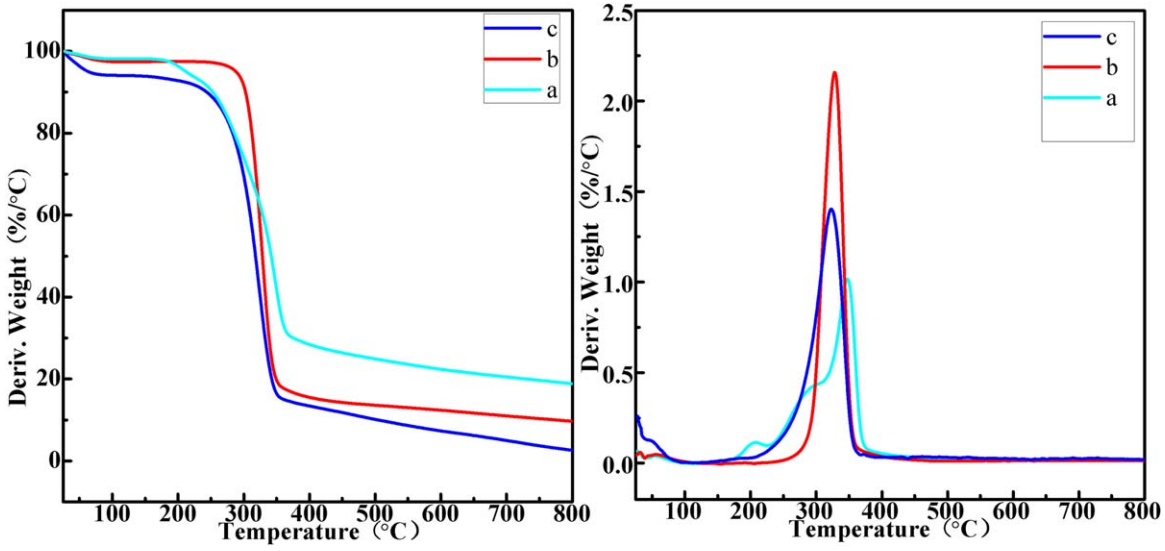

FIG. 5. TGA (left) and DTG (right) curves of the (a) OBP, (b) PBCF, and (c) BCNF. [Color figure can be viewed at wileyonlinelibrary.com]

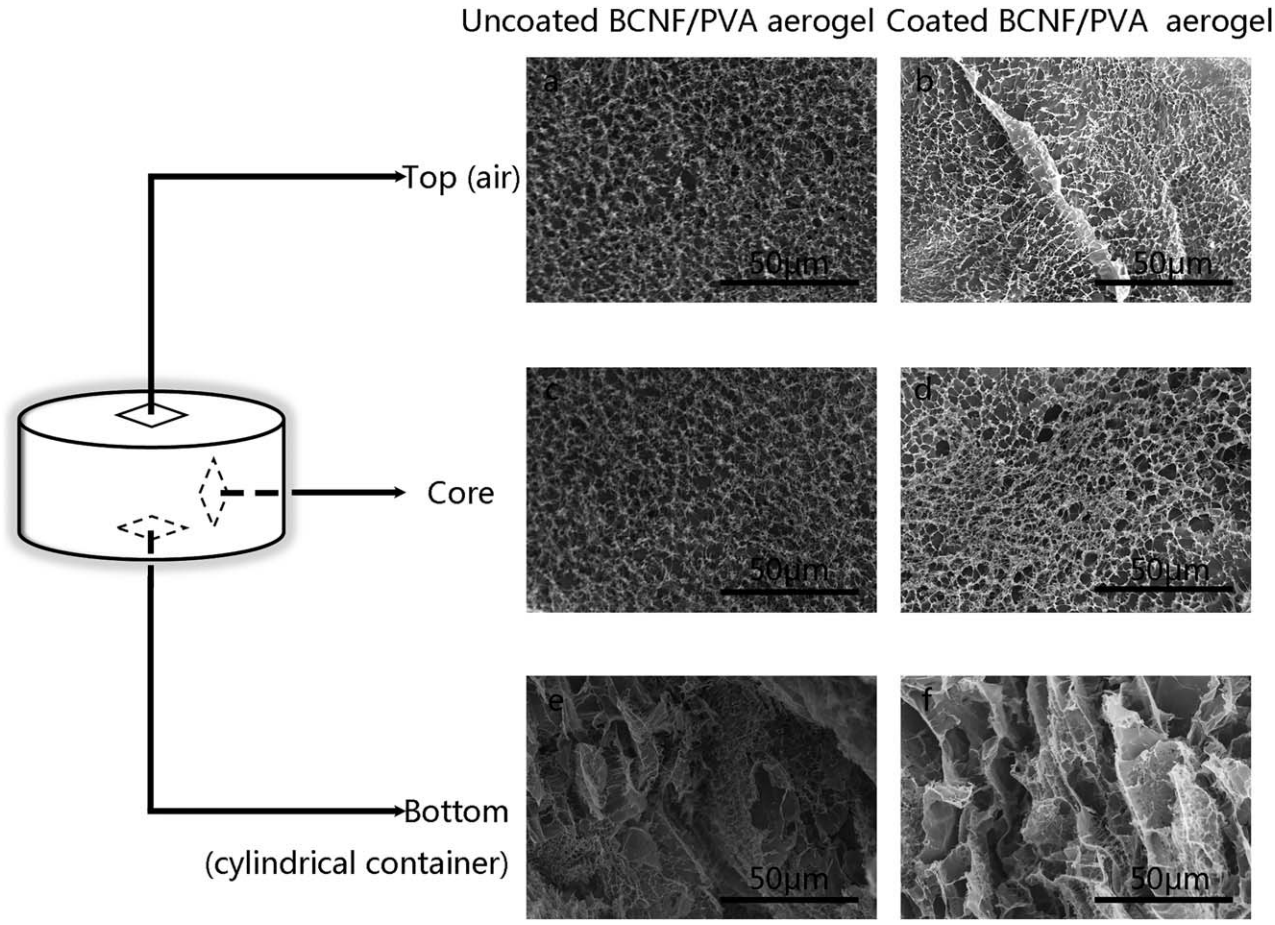

FIG. 6. SEM images of the top (a and b), core (c and d), and bottom (e and f) of BCNF/PVA aerogels with and without silane coating.

the crystallinity of BCNF decreased to 58.73%. The XRD profiles of BCNF demonstrated that the amorphous and crystalline regions were all broken, indicating that the non-crystalline and crystalline celluloses were removed during the ultrasonication. The decreases in the crystallinity may have been due to the faster decline in the proportion of crystalline areas of cellulose moved [47]. The highly crystalline BCNF could be more effective for providing better thermal stability for synthetic materials.

Thermostability Analysis

The thermal stabilities, both TG (in wt%) and derivative thermogravimetric analysis (DTG) (in wt%/°C) curves of the OBP, PBCF, and BCNF, are shown in Fig. 5. An initial weight loss of all of the samples occurred over the temperature range of 25–100°C due to the evaporation of the humidity. Obvious differences were observed among the pyrolysis behaviors of the three samples. Because of the low decomposition temperature of hemicellulose (220–315°C), lignin (25–800°C), and other non-cellulosic segment, the curve of the OBP showed an earlier weight loss that started at ~206°C, which achieved the dominant peak at 348°C on the DTG curve, accounting for the pyrolysis of cellulose (~355°C) [48]. Different to the OBP, the PBCF demonstrated a higher decomposition temperature at 327°C. This phenomenon was caused by the partial removal of hemicellulose and lignin from the

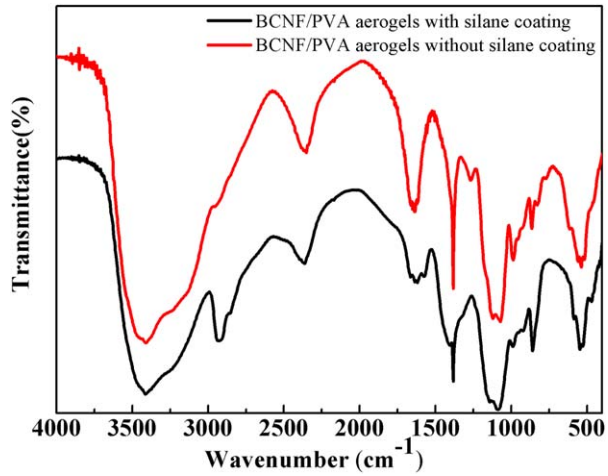

FIG. 7. FTIR spectra of BCNF/PVA aerogels with and without silane coating. [Color figure can be viewed at wileyonlinelibrary.com]

DOI 10.1002/pc

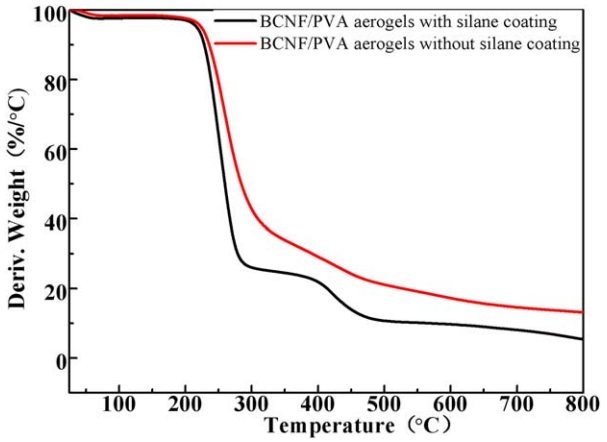

FIG. 8. TGA properties of BCNF/PVA aerogels with and without silane coating. [Color figure can be viewed at wileyonlinelibrary.com]

OBP. The cellulose, consisting of a long polymer of glucose without branches, had a higher crystallinity.

Morphology of BCNF/PVA Aerogels With and Without Silane Coating

The BCNF/PVA aerogels before and after the silane treatment exhibited low densities of 4.7×10^{-2} g cm^{-3} and 4.8×10^{-2} g cm^{-3}, respectively. The SEM was applied to characterize the morphologies of BCNF/PVA aerogels with and without silane coating by taking micrographs of the top, core, and bottom of each sample in Fig. 6. The top and core of both uncoated and coated BCNF/PVA aerogels all exhibited an interconnected, porous structure consisting of a three-dimensional (3D) assembly of nanofilaments randomly (Fig. 6a–d). On the contrary, the textures of the bottom of the BCNF/PVA aerogels with and without silane coating were quite different. These thin sheets resulted from the agglomeration of BCNF when the ice crystals formed during the freezing step [49, 50]. The BCNF/PVA suspension in this layer froze faster than in the core or top of the sample, attributing to the bottom surface of the cylindrical container got in touch directly with freezer. As a result, the ice crystals formed were smaller and a porous structure composed mostly of nanofilaments was acquired with all samples (Fig. 6e and f).

FTIR and TGA of BCNF/PVA Aerogels With and Without Silane Coating

FTIR spectroscopy is very sensitive to modifications of the aerogels upon silane coating treatment. The FTIR spectra of BCNF/PVA aerogels with and without modification are shown in Fig.7. As for the BCNF/PVA aerogels without silane coating, a significant absorption peak was observed at 1141 cm^{-1}, which was ascribed to the C—C stretching mode of PVA and was usually relevant to the crystallinity of PVA. The characteristic absorption bands occurring at 1089, 1014, and 856 cm^{-1} were linked with the stretching of C—O, bending of $–CH_2$ and rocking of –CH, respectively [51]. The absorption peaks at ~790, 1014, and 1269 cm^{-1} were attributed to the characteristic vibrations of Si—O—Si and C—Si asymmetric stretching in C—Si—O units, respectively [52].

The thermal stability measurement of the BCNF/PVA aerogels before and after silane modification was carried out using TGA in nitrogen ranging from 25 to 800°C in Fig. 8. Silane treatment did not alter the thermal stability of the BCNF/PVA aerogels until around 206°C. However, beyond 206°C (up to 800°C), the thermal decomposition temperature of the silane-coated BCNF/PVA aerogel was obviously improved. For instance, the temperatures corresponding to a 54% weight loss were 303.3 and 265.4°C, for the silane-treated and untreated BCNF/PVA aerogels, respectively. This might be because the thermal decomposition of the aerogels was retarded by the silane coating on the porous surface of the BCNF/PVA aerogel [31, 53].

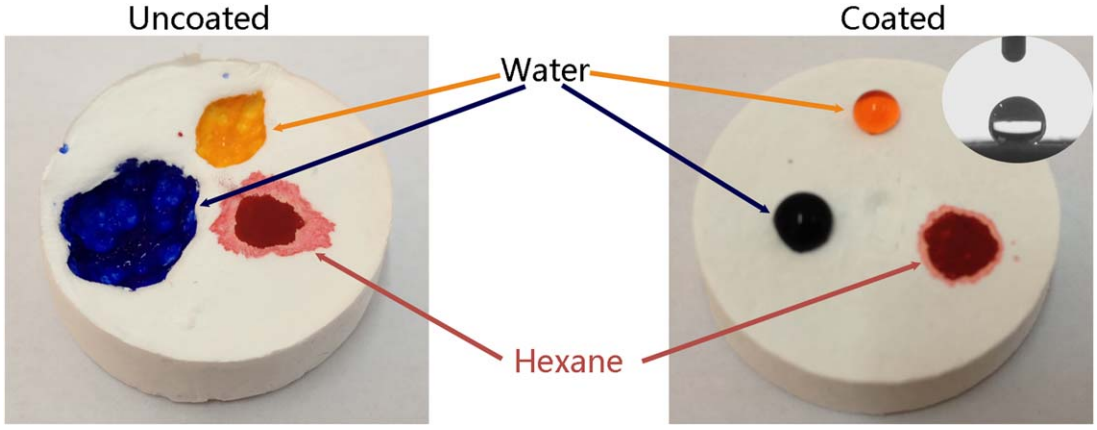

FIG. 9. Illustration of the combined hydrophobic and oleophilic properties of the coated BCNF/PVA aerogels. Inset: photograph of water contact angle of coated BCNF/PVA aerogel. [Color figure can be viewed at wileyonlinelibrary.com]

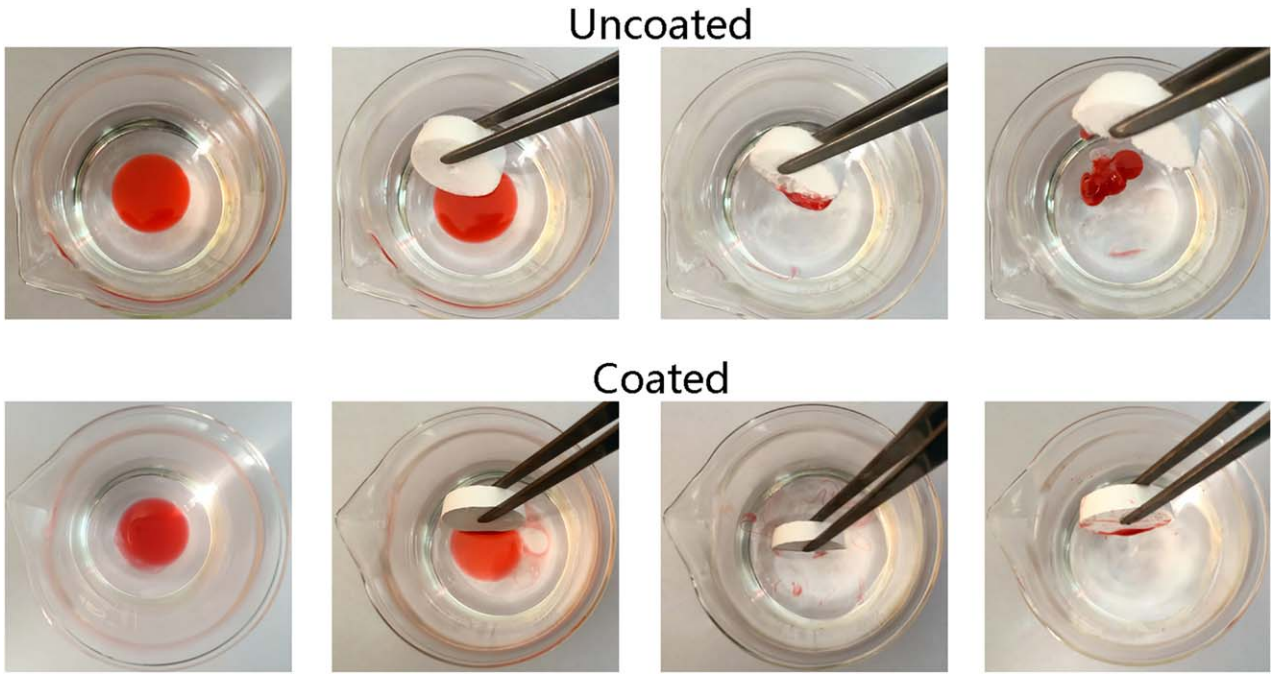

FIG. 10. Removal of a red-dyed pump oil spill from water with the BCNF/PVA aerogel with and without silane coating. [Color figure can be viewed at wileyonlinelibrary.com]

The Wettability of BCNF/PVA Aerogels With and Without Silane Coating

The surface wettability of the BCNF/PVA aerogels with and without silane coating was estimated by investigating the water contact angle at the top or bottom surfaces of the samples. Hexane was dyed red using Sudan III for clear observation. Water was colored by methyl blue and methyl orange. In a preliminary experiment, water and hexane droplets were deposited drop by drop at the top surface of the unmodified and modified BCNF/PVA aerogels (Fig. 9). The untreated sample demonstrated a firm hydrophilicity, as the droplet of the water was immediately absorbed (no WCA could be studied on the surface). On the contrary, the top surface of the modified BCNF/PVA aerogel was highly hydrophobic as the —OH groups of BCNFs were reacted with methyltrichlorosilane to render a hydrophobic character corresponding to a WCA of 136°.

The alternative oil absorption properties of the coated BCNF/PVA aerogel were further illuminated by an adsorption experiment in which pump oil was spilled on the water surface and then brought in contact with the uncoated or coated aerogel (Fig. 10). In comparison, the unmodified aerogel, which quickly saturates with both water and pump oil, was not alternative and lost its initial shape. Whereas the coated aerogel optionally absorbed the pump oil and floated on the surface of water during the test. The mechanical integrity of the coated aerogel was unchangeable, and it could still be used to remove more pump oil.

CONCLUSIONS

The homogenous BCNF ($r = 15.02$ nm) was successfully extracted from moso bamboo using a chemical-ultrasonic process. The prepared BCNF had cellulose I crystal structure similar to that of OBP, with higher crystallinity (58.73%), and higher thermal stability. Hydrophobic and oleophilic BCNF/PVA aerogels were fabricated by an environmental friendly freeze-drying process followed by modification with methyltrichlorosilane using a thermal chemical vapor deposition. The resulting silane-coated BCNF/PVA aerogels had low densities (4.8×10^{-2} g cm^{-3}) and excellent hydrophobicity/oleophilicity (WCA $\approx$ 136°). Furthermore, the BCNF/PVA aerogels were composited of reproducible/inexpensive materials and through facile and green technologies may provide many potential applications in cleaning up oil/chemical spills/leaks.

REFERENCES

1. Q. Zheng, Z. Cai, Z. Ma, and S. Gong, *ACS Appl. Mater. Interfaces*, **7**, 3263 (2015).
2. M.A.B. Meador, S. Wright, A. Sandberg, B.N. Nguyen, F.W. Van Keuls, C.H. Mueller, R. Rodríguez-Solís, and FlA. Miranda, *ACS Appl. Mater. Interfaces*, **4**, 6346 (2012).
3. F. Fischer, A. Rigacci, R. Pirard, S. Berthon-Fabry, and P. Achard, *Polymer*, **47**, 7636 (2006).
4. J. Gross, J. Fricke, and L. Hrubesh, *J. Acoust. Soc. Am.*, **91**, 2004 (1992).
5. E. Guilminot, F. Fischer, M. Chatenet, A. Rigacci, S. Berthon-Fabry, P. Achard, and E. Chainet, *J. Power Sources*, **166**, 104 (2007).
6. R. Baetens, B.P. Jelle, and A. Gustavsen, *Energ. Buildings*, **43**, 761 (2011).
7. S.H. Wu, C.Y. Mou, and H.P. Lin, *Chem. Soc. Rev.*, **42**, 3862 (2013).

 DOI 10.1002/pc

8. R. Pekala, J. Farmer, C. Alviso, T. Tran, S. Mayer, J. Miller, and B. Dunn, *J. Non-Cryst. Solids*, **225**, 74 (1998).
9. Y. Lu, Q. Sun, D. Yang, X. She, X. Yao, G. Zhu, Y. Liu, H. Zhao, and J. Li, *J. Mater. Chem.*, **22**, 13548 (2012).
10. V.K. Thakur, M.K. Thakur, P. Raghavan, and M.R. Kessler, *ACS Sustain. Chem. Eng.*, **2**, 1072 (2014).
11. V.K. Thakur, M.K. Thakur, and R.K. Gupta, *Int. J. Polym. Anal. Chem.*, **19**, 256 (2014).
12. Z. Jiang, Z. Liu, B. Fei, Z. Cai, and Y. Yu, *J. Anal. Appl. Pyrol.*, **94**, 48 (2012).
13. J. Cai, L. Zhang, J. Zhou, H. Qi, H. Chen, T. Kondo, X. Chen, and B. Chu, *Adv. Mater.*, **19**, 821 (2007).
14. V.K. Thakur, Green Composites From Natural Resources, CRC Press Taylor & Francis, Boca Raton, FL, USA (2013).
15. V.K. Thakur, Cellulose-Based Graft Copolymers: Structure and Chemistry, CRC Press Taylor & Francis, Boca Raton, FL, USA (2015).
16. V.K. Thakur and M.K. Thakur, *Carbohydr. Polym.*, **109**, 102 (2014).
17. Y. Habibi, L.A. Lucia, and O.J. Rojas, *Chem. Rev.*, **110**, 3479 (2010).
18. V.K. Thakur, Nanocellulose Polymer Nanocomposites: Fundamentals and Applications, Wiley: Salem, Massachusetts (2014).
19. V.K. Thakur and M.K. Thakur, Eco-Friendly Polymer Nanocomposites: Chemistry and Applications, Springer, New Delhi (2015).
20. A. Alemdar and M. Sain, *Bioresour. Technol.*, **99**, 1664 (2008).
21. S. Iwamoto, A. Nakagaito, and H. Yano, *Appl. Phys. A*, **89**, 461 (2007).
22. H. Yano, J. Sugiyama, A.N. Nakagaito, M. Nogi, T. Matsuura, M. Hikita, and K. Handa, *Adv. Mater.*, **17**, 153 (2005).
23. S. Elazzouzi-Hafraoui, Y. Nishiyama, J.L. Putaux, L. Heux, F. Dubreuil, and C. Rochas, *Biomacromolecules*, **9**, 57 (2007).
24. M. Pääkkö, M. Ankerfors, H. Kosonen, A. Nykänen, S. Ahola, M. Österberg, J. Ruokolainen, J. Laine, T. Larsson, and O. Ikkala, *Biomacromolecules*, **8**, 1934 (2007).
25. T. Saito, M. Hirota, N. Tamura, S. Kimura, H. Fukuzumi, L. Heux, and A. Isogai, *Biomacromolecules*, **10**, 1992 (2009).
26. S. Xiao, R. Gao, Y. Lu, J. Li, and Q. Sun, *Carbohydr. Polym*, **119**, 202 (2015).
27. W. Chen, H. Yu, Y. Liu, P. Chen, M. Zhang, and Y. Hai, *Carbohydr. Polym*, **83**, 1804 (2011).
28. P.C.F. Tischer, M.R. Sierakowski, H. Westfahl Jr, and C.A. Tischer, *Biomacromolecules*, **11**, 1217 (2010).
29. Y. Lu, Q. Sun, X. She, Y. Xia, Y. Liu, J. Li, and D. Yang, *Carbohydr. Polym*, **98**, 1497 (2013).
30. L. Chen, D. Rende, L.S. Schadler, and R. Ozisik, *J. Mater. Chem. A*, **1**, 3837 (2013).
31. Q. Zheng, Z. Cai, and S. Gong, *J. Mater. Chem. A*, **2**, 3110 (2014).
32. J. Han, T. Lei, and Q. Wu, *Cellulose*, **20**, 2947 (2013).
33. M.K. Thakur, A.K. Rana, L. Yang, A.S. Singha, and V.K. Thakur, Surface Modification of Biopolymers, Wiley, New Jersey (2015).
34. J.N. Coleman, U. Khan, W.J. Blau, and Y.K. Gun'Ko, *Carbon*, **44**, 1624 (2006).
35. K. Song, Y. Zhang, J. Meng, E.C. Green, N. Tajaddod, H. Li, and M.L. Minus, *Materials*, **6**, 2543 (2013).
36. K. Abe, and H. Yano, *Cellulose*, **16**, 1017 (2009).
37. J. Gu and Y.L. Hsieh, *ACS Appl. Mater. Interfaces*, **7**, 4192 (2015).
38. K. Okubo, T. Fujii, and Y. Yamamoto, *Compos. Part A*, **35**, 377 (2004).
39. A.V.R. Prasad and K.M. Rao, *Mater. Des.*, **32**, 4658 (2011).
40. A. Sluiter, B. Hames, R. Ruiz, C. Scarlata, J. Sluiter, D. Templeton, and D. Crocker, *Lab. Anal. Proced.* **1617** (2008).
41. H. Sehaqui, Q. Zhou, and L.A. Berglund, *Compos. Sci. Technol.*, **71**, 1593 (2011).
42. M.G. Thomas, E. Abraham, P. Jyotishkumar, H.J. Maria, L.A. Pothen, and S. Thomas, *Int. J. Biol. Macromol.*, **81**, 768 (2015).
43. M. Sain and S. Panthapulakkal, *Ind. Crop. Prod.*, **23**, 1 (2006).
44. R. Sun, J. Tomkinson, Y. Wang, and B. Xiao, *Polymer*, **41**, 2647 (2000).
45. N. El Miri, K. Abdelouahdi, M. Zahouily, A. Fihri, A. Barakat, A. Solhy, and M. El Achaby, *J. Appl. Polym. Sci.*, **22**, 132 (2015).
46. Y. Nishiyama, P. Langan, and H. Chanzy, *J. Am. Chem. Soc.*, **124**, 9074 (2002).
47. W. Li, X. Zhao, Z. Huang, and S. Liu, *J. Polym. Res.*, **20**, 1 (2013).
48. H. Yang, R. Yan, H. Chen, D.H. Lee, and C. Zheng, *Fuel*, **86**, 1781 (2007).
49. A.J. Svagan, M.A. Samir, and L.A. Berglund, *Adv. Mater.*, **20**, 1263 (2008).
50. H. Jin, Y. Nishiyama, M. Wada, and S. Kuga, *Colloids Surf. A*, **240**, 63 (2004).
51. D. Liu, X. Sun, H. Tian, S. Maiti, and Z. Ma, *Cellulose*, **20**, 2981 (2013).
52. Q. Zhu, Y. Chu, Z. Wang, N. Chen, L. Lin, F. Liu, and Q. Pan, *J. Mater. Chem. A*, **1**, 5386 (2013).
53. A.N. Frone, D.M. Panaitescu, D. Donescu, C.I. Spataru, C. Radovici, R. Trusca, and R. Somoghi, *BioResources*, **6**, 487 (2011).